Supporting Information for:

Secondary organic aerosol from OH-initiated oxidation of mixtures of d-limonene and β-myrcene

Sijia Liu[1], Tommaso Galeazzo[1], Richard Valorso[3], Manabu Shiraiwa[1], Celia L. Faiola[1,2], and Sergey A Nizkorodov[1]*

1. Department of Chemistry, University of California Irvine, Irvine, California 92697, United States

2. Department of Ecology and Evolutionary Biology, University of California Irvine, Irvine, California 92697, United States

3. Univ Paris Est Creteil and Université Paris Cité, CNRS, LISA, F-94010 Créteil, France

Summary: 20 pages, additional information about experiments and data analysis, 11 figures, 2 tables, and a list of supporting references.

Table of Contents

VOC Sampling and GC-MS Analysis

After VOC concentrations in the chamber had stabilized, air samples were taken using multi-bed stainless steel adsorbent cartridges (Carbograph and Tenax TA; Markes International) connected to an air sampling pump (Sensidyne GilAir Plus) with a flow rate of 0.25 L min^{-1} for 8 min. Cartridges were stored at room temperature and analyzed within 32 h of collection via a thermal-desorption (TD, Markes International, TD-100xr) coupled to a gas-chromatography mass spectrometry instrument (GC-MS, Agilent GC 7890B, MSD 5973). The tube desorption occurred at a temperature of 250 ℃ with a nitrogen flow of 10 mL min^{-1}. The VOC was held at a cold trap at -10 ˚C. The VOC was heated to 300 ˚C to be transferred to the GC. The column flow was 2.5 mL min^{-1}. The GC column held 40˚C for 2 min, then ramped to 210 ℃ at a rate of 10 ℃ min^{-1}, followed by a ramp to 275 ℃ at 30 ℃ min^{-1} and held for 2 min.

UPLC-HRMS and Molecular Assignments

SOA filter samples were extracted into approximately 5 mL of a solvent mixture containing 50 vol% acetonitrile in water, with the actual extraction volume adjusted based on the mass of the collected SOA. This approach ensured that the concentrations of all SOA extracts were maintained at approximately 250 μg/mL for all experiments. Blanks were prepared using the same solvent to extract empty filters for comparative analysis. The extracts were analyzed using an UPLC-ESI-HRMS setup (Thermal Scientific) consisting of a Vanquish Horizon UPLC module coupled to a Q Exactive Plus Orbitrap analyzer, equipped with heated-inlet electrospray ionization (HESI) ion source. The UPLC was equipped with a Phenomenex Luna Omega Polar C_{18} column with the dimension of 150 × 2.1 mm (1.6 μm particles and 100 Å pores) and operated under 30 ℃, and the eluents were composed of HPLC-optima grade water (eluent A) and acetonitrile (eluent B) (Sigma-Aldrich) with 0.1% HPLC grade formic acid (Sigma-Aldrich). HRMS was run under both positive and negative electrospray ionization (ESI) modes. The elution gradient began with 95% eluent A for the first 3 min, then transitioned linearly to 95% eluent B over the next 11 min, maintained this composition for 2 min, and finally returned to 95% eluent A for the last 6 min. The data were extracted using Thermo Scientific FreeStyle 1.6 by integrating mass spectra over retention times from 2-16 min. Gaussian smoothing was

applied to the chromatograms within FreeStyle. Data were processed using an open-source molecular formula assignment package, MFAssignR,[1] where the retention-time-integrated mass spectra peaks of blank and SOA samples were clustered within a tolerance of ± 5 ppm, and the peaks with higher abundance in blank spectra were removed. The remaining peaks of SOA samples were assigned to formulae $C_xH_yO_z$ assuming an accuracy of ± 5 ppm, and the ambiguous peaks were removed. Neutral formulae were determined based on the ionization mechanism, and peaks of both positive and negative ion modes were combined to create a list of detected molecular formulae.

GECKO-A Mechanism Modeling

GECKO-A implements the latest Structure Activity Relationships (SARs) developments to treat the chemistry of organic compounds, including the following: oxidation of VOCs by the dominant atmospheric oxidants (OH, O_3, and NO_3), peroxy alkyl chemistry, peroxy acyl chemistry, and alkoxy chemistry.[2] Peroxy acyl chemistry includes RO_2 permutation reactions, and cross-species RO_2 reactions leading to R(OH) and R(=O) formation. We should note that at this stage of model development, GECKO-A does not include RO_2 + RO_2 reactions leading to ROOR or ROOR' dimers formation, autoxidation in the gas phase, or any particle-phase reactions. In our simulations, semi-volatile species vapor pressures were estimated via the approach by Nannoolal et al.[3] The generator assumes that species with vapor pressures below 10^{-13} atm have low enough volatility to undergo complete gas-particle partitioning to the condensed phase as described by Valorso et al.[4] Therefore, for these species, no gas phase chemistry is considered.

The GECKO-A generated mechanism was integrated in a box model to simulate the formation of SOA for the chamber experiments conditions, following the approach outlined in La et al.[5] The box model does not account for particle nucleation, but seed particles were not used in chamber experiments. As a workaround, we approximated the initial nucleation process in our simulations by introducing seed particles with a particle radius of 5 nm and a concentration of 10^4 particles cm^{-3}.[6,7] The temperature was kept constant at 293.15 K, the pressure was set to 1 atm, and the RH was maintained at 50%, 50.6%, and 47.6% for the simulations of oxidation of d-limonene, β-myrcene, and their mixture respectively. Photolysis frequencies were determined using absorption cross sections,

quantum yields, and the photonic flux of blacklight lamps, following the methodology outlined in Aumont et al.[8] and Valorso et al.[4] To replicate the measured [OH] concentrations in the chamber, we set the OH concentration for d-limonene, β-myrcene, and the mixture simulations at 3.8×10^6, 1.9×10^6, and 2.9×10^6 molecules cm^{-3}, respectively. Each simulation was carried out for a duration of 2 h, and the time evolution of species concentration was calculated using a solver for stiff differential equations.[9,10] According to the simulations, the concentrations of HO_2 were 1.3×10^8, 3.8×10^8, 7.5×10^7 molec cm^{-3} for d-limonene, β-myrcene and the mixture case, respectively, and the combined concentrations of all RO_2 radicals (excluding HO_2) were 4.4×10^9, 9.7×10^9, 1.1×10^{10} molec cm^{-3}, respectively, after 2 h of running the simulation. The box model considers the kinetics of mass transfer for organic species between the gas and particle phases, and reversible deposition of gas-phase species to the walls as in La et al. [5] The partitioning process adheres to Raoult's law for equilibrium, and the partitioning kinetics are described by the gas-particle mass transfer coefficient using the Fuchs-Sutugin approach.[11]

Comparison with the GECKO-A prediction

The significant overlap in the distribution of molecular formulas across different SOA systems (Figure 2 in the manuscript), combined with direct observation of isomers in EICs (Figure 4 in the manuscript), suggested the formation of multiple isomeric products in the OH-initiated oxidation of d-limonene SOA, β-myrcene, and its mixtures. We used GECKO-A to assess the extent of formation of different isomers under our experimental conditions. It is crucial to emphasize that we are not comparing the GECKO-A predicted structures with the observed mass spectra directly, but rather the goal is to obtain qualitative information about isomeric complexity of the oxidation products expected from these systems.

GECKO-A tracks simulated compounds using structural formulae (*e.g.* $CH_3CH_2CH_2CH_3$ for butane). Each structural isomer has the same chemical formula but a unique structural formula. We focused here on the top 2000 abundant species in SOA simulated by GECKO-A at the end of each simulation to identify any unique compounds formed in the mixed VOC oxidation system compared to the single component systems. To compare

GECKO-A results with the HRMS data, we first condensed structural formula to chemical formulae, and found significant overlap in the predicted formulae for d-limonene SOA, β-myrcene, and mixed cases (Figure S1a), similar to what was observed in the experimental HRMS data (Figure 2 in the manuscript).

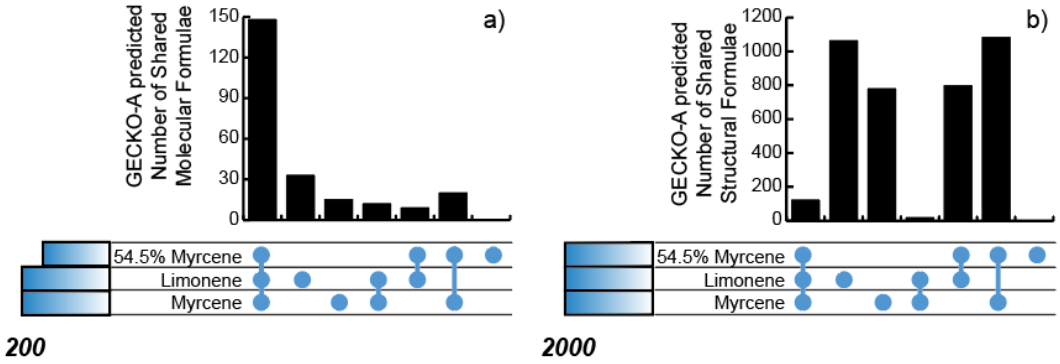

Figure S1. UpSet plots for comparing overlap between a) GECKO-A predicted chemical formulas across the three systems, and (b) GECKO-A predicted structural formulae of 54.5% β-myrcene (mixture), β-myrcene, and d-limonene SOA. The horizontal bar charts at the bottom left display the total number of unique chemical formulae or structural formulae in each system. The matrix illustrates the intersections between systems through filled blue circles. The vertical bar chart quantifies the number of these intersections. Each data point was only counted once.

However, this overlap is misleading because the same formulae for β-myrcene and d-limonene oxidation products actually correspond to different isomeric compounds. In fact, we found that a single GECKO-A predicted molecular formula could correspond to up to 78 distinct isomers (Figure S5). When we compared the predicted species from GECKO-A (Figure S1b), the apparent overlap from the three precursor systems became far less pronounced, only ~100 species, highlighting the immense chemodiversity of SOA composition and demonstrating that the observed mass spectra hide a great amount of chemical complexity. We then compared structural formulae among the single precursor system and mixture system (Figure S1b). Given the enhanced chemodiversity in the mixture SOA, certain compounds predicted in individual precursors might be absent from our mixture SOA product predictions, since we limited our analysis to the top 2,000 most abundant compounds (Figure S2, which explained the large portion of distinct compounds for the single precursor SOA in Figure S1b. Surprisingly, no structural formula appeared

to be unique to the mixed SOA case, supporting the importance of other reaction routes in the formation of characteristic cross-reaction products representing the SOA mixture.

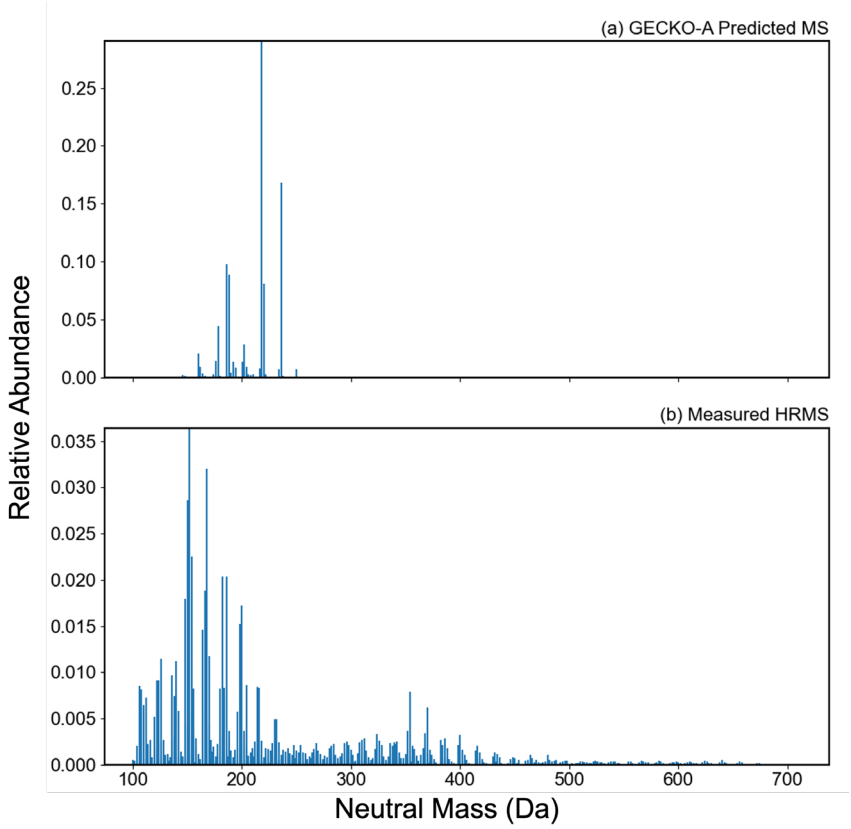

Figure S2. Comparative analysis of GECKO-A predicted and observed mass spectra of 54.5 % β-myrcene SOA. (a) The GECKO-A predicted mass spectrum showcases the predicted relative abundance of various molecular masses based on the simulated atmospheric reactions. (b) The observed high-resolution mass spectrum from measurements. The large shfit in the center of the GECKO-A envelope (around 200 Da) and observed monomeric products (around 160 Da) is believed to be due to the significiant fragmentation of SOA compounds in the ion source. Note that GECKO-A cannot predict the dimeric products.

Takeuchi et al. (2022) proposed that most of cross-species formed in mixed reaction systems are dimers formed in the gas phase by RO_2 + $R'O_2$ reactions or oligomers formed in the particle phase by reactions of condensed monomeric species.[12] It is important to note that the GECKO-A model does not consider RO_2 + $R'O_2$ reactions leading to dimer

formation, nor does it account for any particle phase chemistry. However, the GECKO-A generator does take into account RO_2 + $R'O_2$ reactions resulting in the formation of ROH + R'(=O)H closed shell and RO + R'O radical products.[8] In all of our box model simulations, the dominant species in the particle phase are multi-functional ROH and R(=O)H compounds that possess reactive sites for oligomerization in the particle phase (e.g., by hemiacetal formation). According to the reaction mechanism proposed by Takeuchi et al. (2022) for d-limonene and α-pinene, multifunctional compounds serve as precursors for oligomers and cross-species compounds with higher molecular mass.[12] To gain a better understanding of the extent to which these reactions contribute to the formation of cross-species products or larger oligomers in SOA, particle phase chemistry should be explicitly included in the future models.

Viscosity Estimation

The glass transition temperature (T_g) is defined as the temperature at which the phase of SOA changes from a viscous semisolid state to a glassy solid state.[13–15] Material viscosity can be predicted from T_g. DeRieux et al. demonstrated that the molecular compositions of SOA from analyzed mass spectra can be used to estimate the T_g of the SOA material:

$$T_g = (n_C^0 + \ln(n_C))b_C + \ln(n_H)\, b_H + \ln(n_C)\ln(n_H)\, b_{CH} + \ln(n_O)\, b_O + \ln(n_C)\ln(n_O) b_{CO},$$

where n_C^0 stands for reference carbon number, while b_C, b_H, b_{CH}, b_O, and b_{CO} represent the contribution of each atom to T_g, and the values are listed in Table S1.[16,17]

Table S1. **Classes of chemical compounds and saturation mass concentration parameterization described by Li et al. and DeRieux et al.**[16,17]

Classes	n_C^0	b_C	b_H	b_{CH}	b_O	b_{CO}
CH	1.96	61.99	-113.33	28.74		
CHO	12.13	10.95	-41.82	21.61	118.96	-24.38

The $T_{g,\,org}$ values for SOA mixture in dry settings were estimated with a linear relationship using Gordon-Taylor method, [18,19] assuming the Gordon-Taylor constant (k_{GT}) of 1:[19]

$$T_g = \sum_i w_i T_g$$

Here, w_i denotes the mass fraction of component 'i'. For our studies, the relative abundance of each compound was represented as [A_i], calculated from the following method from Nguyen et al. (2013):[20]

$$[A_i] = \frac{I_i}{(H/C)_i \times M_i}$$

Via converting I_i to A_i, we took consideration of the influence of molecular weight (M_i) and the degree of saturation, represented by $(H/C)_i$ ratio on ionization efficiency.

Under humid conditions, SOA particles take up water, altering the T_g, and the T_g of water-organic mixture can be represented by $T_{g,(worg)}$ using Gordon–Taylor equation:[21]

$$T_{g\,(w_{org})} = \frac{\left(1 - w_{org}\right) T_{g,w} + \frac{1}{k_{GT}} w_{org}\, T_{g,org}}{\left(1 - w_{org}\right) + \frac{1}{k_{GT}} w_{org}}$$

where w_{org} represents the mass fraction of the organic components, $T_{g,w}$ stands for the glass transition temperature of water ($T_{g,w}$ = 136 K), k_{GT} stand for Gordon-Taylor constant and set to 2.5.[21,22]

The effective hygroscopicity parameter κ, assumed to be 0.1 derived from previous measurement,[23,24] was used to calculate the mass concentration of SOA (m_{SOA}) and water (m_{H2O}):[25]

$$m_{H_2O} = \frac{\kappa \rho_w m_{SOA}}{\rho_{SOA}(\frac{1}{a_w} - 1)}$$

ρ_w and ρ_{SOA} represent density of water (1.0 g cm^{-3}) and density of SOA (1.4 g cm^{-3}) respectively, and a_w stands for water activity and is calculated as a_w=RH/100.[26]

The temperature-dependence of viscosity was calculated using the Vogel-Fulcher-Tammann (VFT) equation:

$$\log(\eta) = -5 + 0.434\,\frac{T_0 D_f}{T - T_0}$$

where T_0 represents the Vogel temperature, which can be calculated using $T_0 = \frac{39.17\,T_g}{D_f + 39.17}$. D_f is the fragility parameter, representing the deviation from Arrhenius behavior, and was assumed to be 10.[17]

Volatility Estimation

To estimate volatility distribution of SOA compounds, we used the parameterization developed by Li et al. to predict pure compound saturation mass concentrations (C_0): [27]

$$log_{10}C_0 = (n_C^0 - n_c)b_c - n_O b_O - 2\frac{n_C n_O}{n_C + n_O}b_{CO}$$

In this equation, n_C^0 is the reference carbon number, and n_c and n_O denote for the number of carbon and oxygen, correspondingly. The parameters are included in Table S2. Note that this formula-based estimation is reasonable for application to a mixture of isomers but creates uncertainty commensurate with the lack of structural information.[28]

Table S2. **Classes of chemical compounds and saturation mass concentration parameterization described by Li et al..**[29]

Classes	n_C^0	b_C	b_O	b_{CO}
CH	23.8	0.48861		
CHO	22.66	0.4481	1.656	-0.7790

SOA Yield

The effective SOA mass yield (Y) was calculated by normalizing the condensed organic particle mass by the mass of reacted monoterpenes (Table 1):

$$Y = \frac{\Delta C_{OA}}{\Delta VOC}$$

More specifically, ΔC_{OA} is the condensed organic aerosol mass (μg/m^3) and ΔVOC denotes the mass of total precursor reacted in the smog chamber (μg/m^3). ΔC_{OA} was calculated based on SMPS integrated particle volume with an assumed density of 1.2

g/cm^3.[30–32] ΔVOC was calculated from PTR-ToF-MS real-time data, which was calibrated against the offline TD-GC-MS measurements.

Supporting Figures and Tables

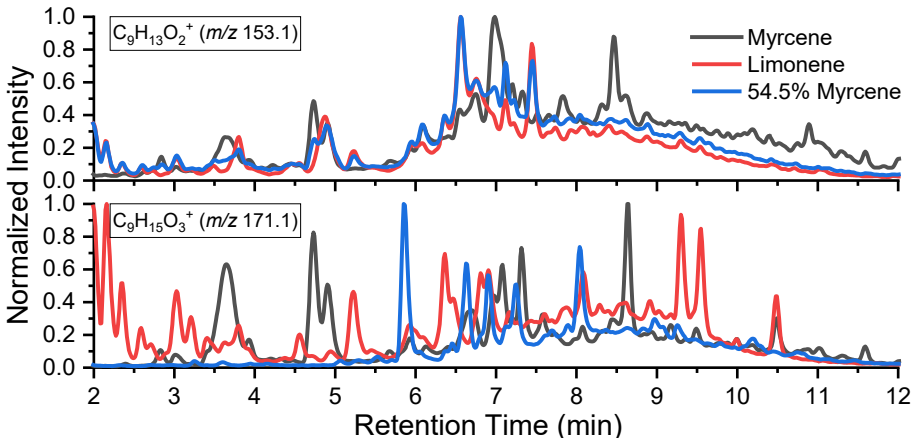

Figure S3. The EICs of major C_9 ions, a) $C_9H_{13}O_2^+$ and b) $C_9H_{15}O_3^+$ observed in β-myrcene, d-limonene and 54.5% binary mixture SOA. The appearance of these ions across a wide range of retention times implies that they form in fragmentation of other SOA compounds.

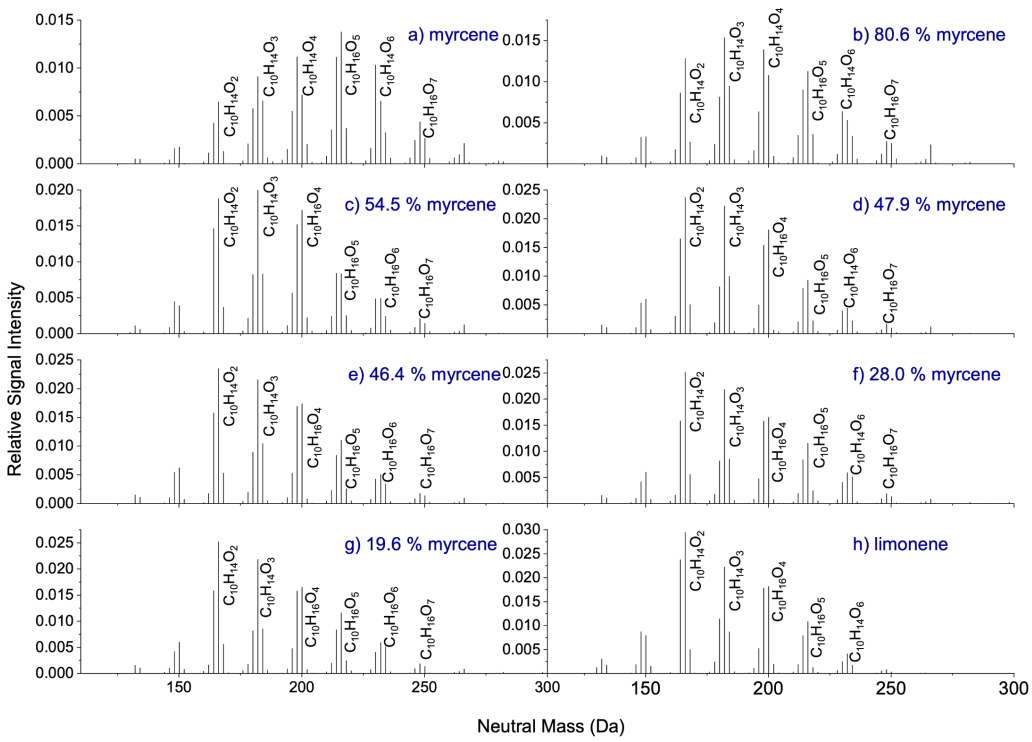

Figure S4. The mass spectra including the C10 families of single and mixture SOA. Other CHO families have been omitted for clarity. Note that the intensity scales are different.

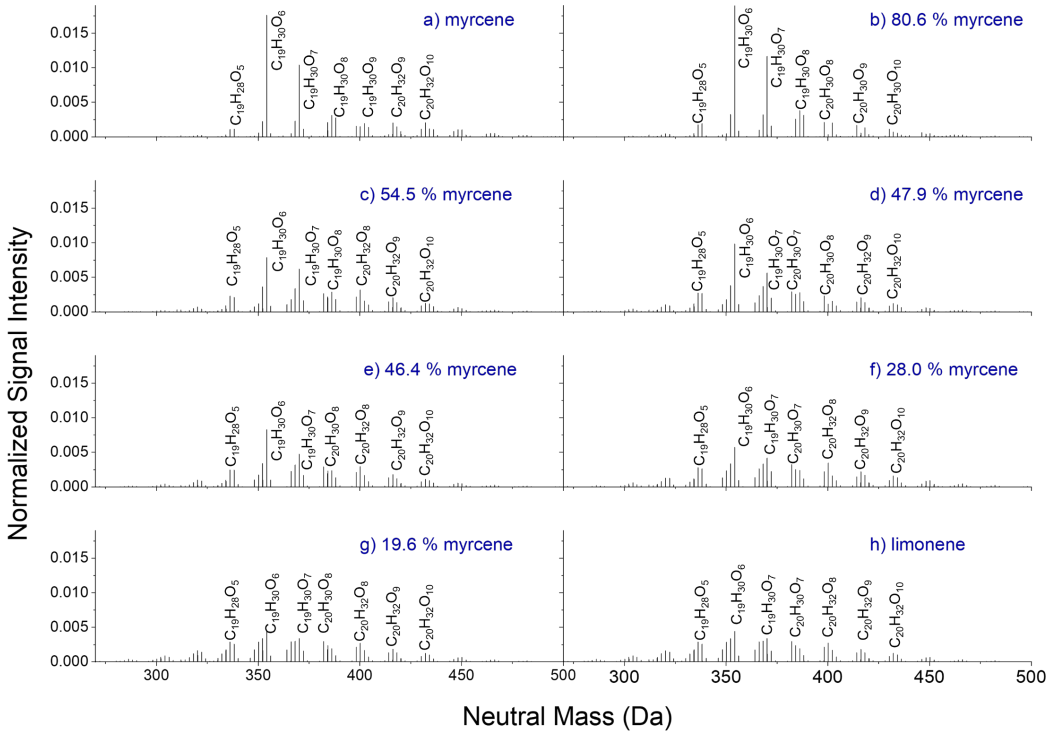

Figure S5. The mass spectra including the C19 and C20 families of single and mixture SOA. Other CHO families have been omitted for clarity. Note that the intensity scales are different.

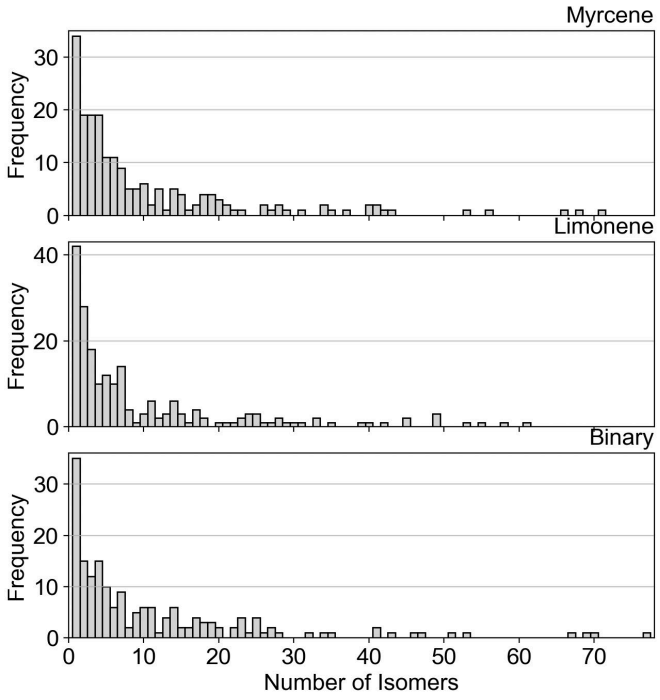

Figure S6 Comparison of Isomer Counts Distribution for β-myrcene, d-limonene, and binary (54.5% β-myrcene). Each plot illustrates the frequency distribution of isomer counts for the respective compound as simulated by the GECKO-A model. The x-axis represents the number of isomers per unique molecular formula, while the y-axis indicates the frequency of such occurrences. The most common number of isomers is 1.

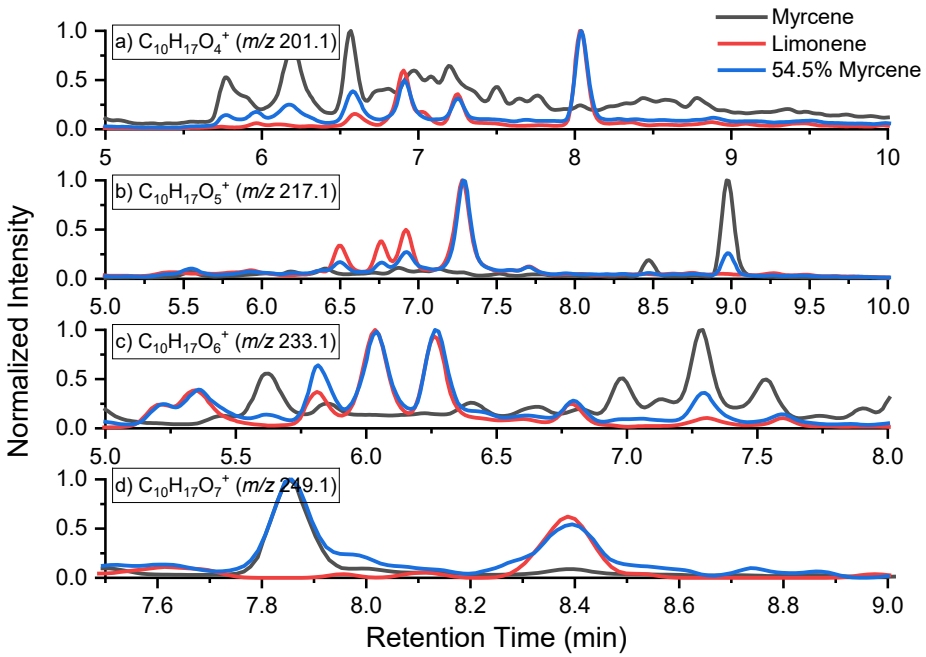

Figure S7. The EICs of a) $C_{10}H_{17}O_4^+$, b) $C_{10}H_{17}O_5^+$, c) $C_{10}H_{17}O_6^+$, and d) c) $C_{10}H_{17}O_7^+$ of d-limonene, β-myrcene, and 54.5% β-myrcene mixture.

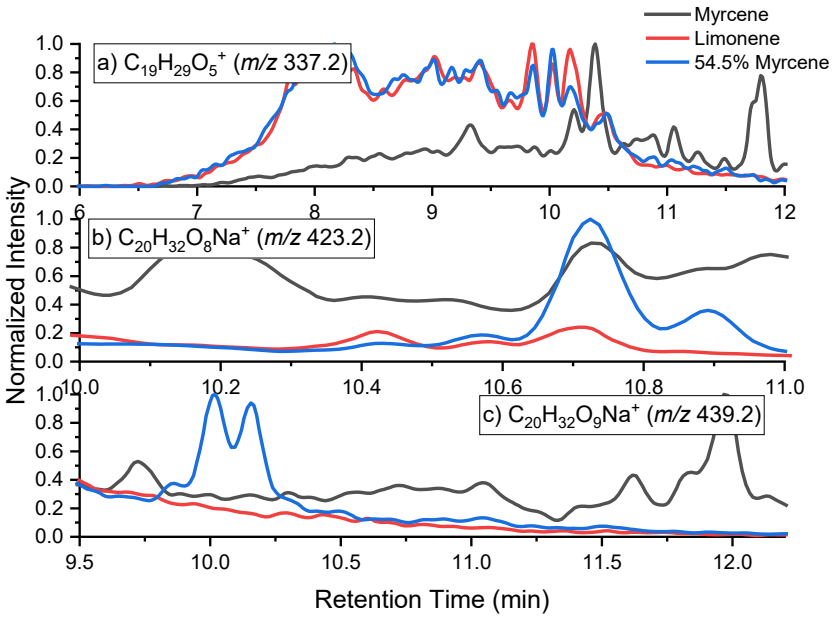

Figure S8. The EICs of a) $C_{19}H_{29}O_5^+$, b) $C_{20}H_{32}O_8Na^+$, and c) $C_{20}H_{32}O_9Na^+$ of d-limonene, β-myrcene, and 54.5% β-myrcene mixture. B) and C) indicated potential formation of distinct isomer in mixture SOA.

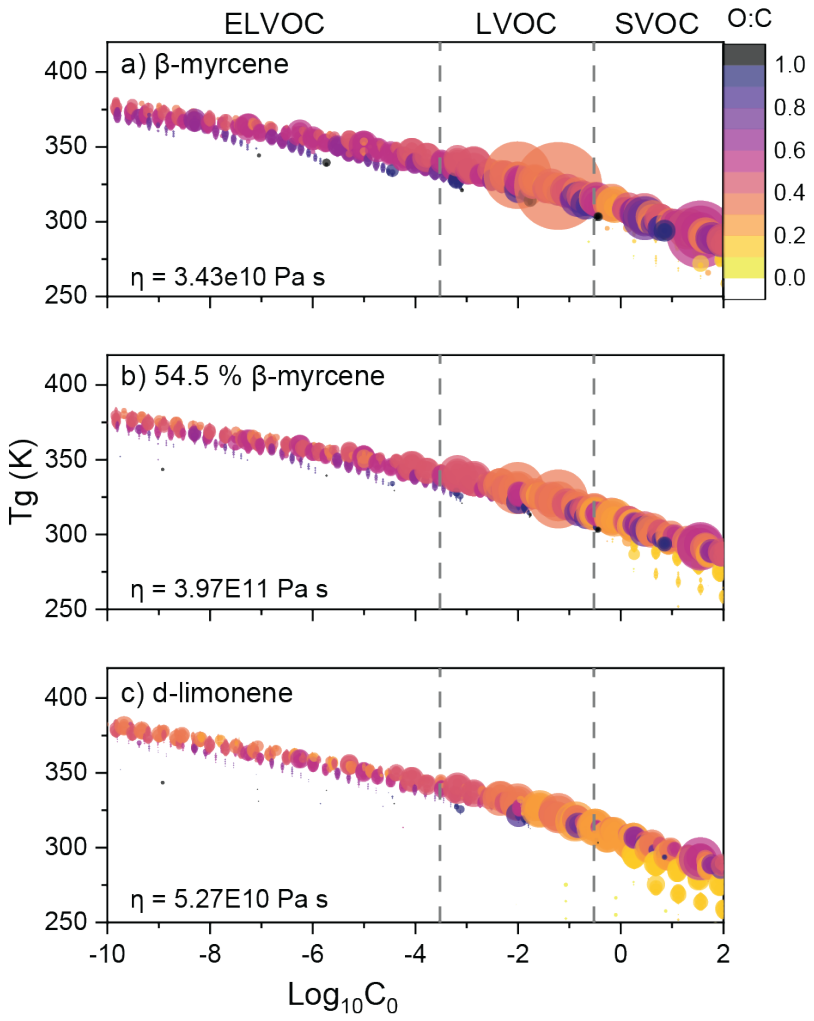

Figure S9. The estimated glass transition temperature T_g (K) and $\log_{10}C_0$ from assigned peak from HRMS of SOA corresponding to different fractional reactivity of β-myrcene: a) 100% (pure β-myrcene SOA), b) 54.5 %, and c) 0 % (pure d-limonene SOA). The size of each circle represents the relative abundance of the signal in the mass spectrum. The color scale represents the O:C ratio, with the darker color corresponding to higher O:C ratio. The labels include the overall $T_{g,\ org}$ for the SOA mixture, as well as the corresponding SOA viscosity (η) values, calculated for RH = 50% and room temperature (~23 ˚C). The LVOCs are excluded from the estimation of viscosity due to their low likelihood of being in the particle phase.

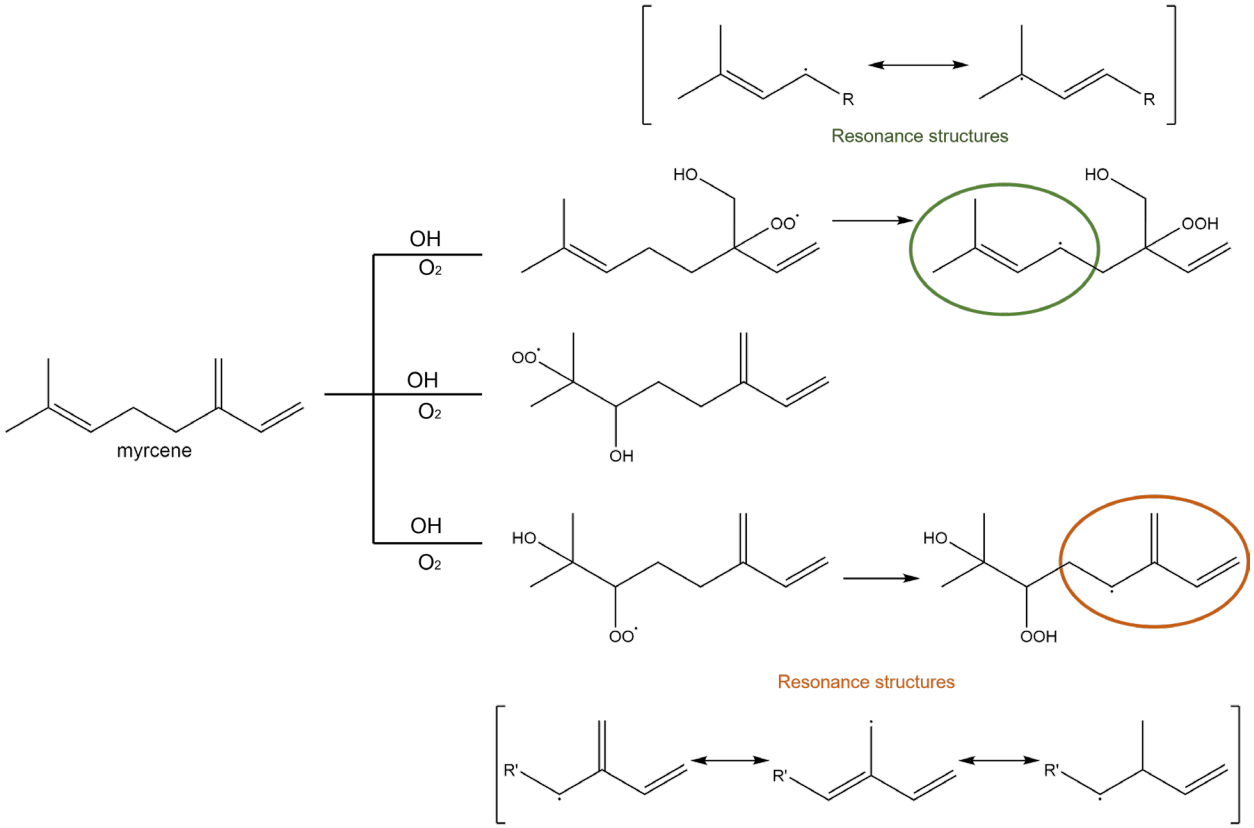

Figure S10. The proposed mechanism of β-myrcene with OH and O_2. The diagram illustrates the flexibility of RO_2 radicals from β-myrcene. Possible resonance structures were included.

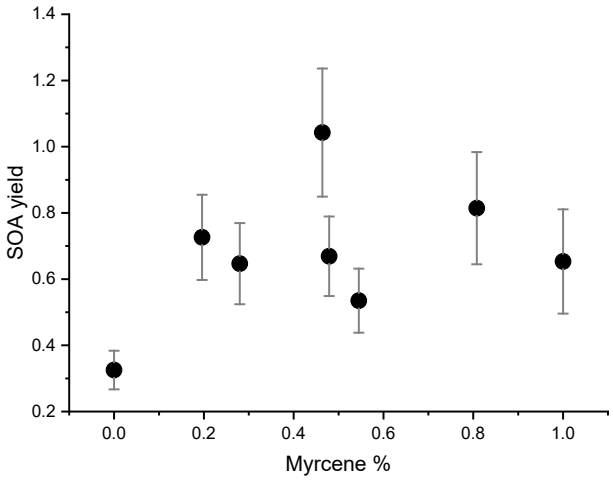

Figure S11. yield (y-axis) against the fraction of OH reactivity due to β-myrcene (x-axis) for various binary mixtures.

References

(1) Schum, S. K.; Brown, L. E.; Mazzoleni, L. R. MFAssignR: Molecular Formula Assignment Software for Ultrahigh Resolution Mass Spectrometry Analysis of Environmental Complex Mixtures. *Environ Res* **2020**, *191*, 110114. https://doi.org/10.1016/J.ENVRES.2020.110114.

(2) Jenkin, M. E.; Valorso, R.; Aumont, B.; Rickard, A. R. Estimation of Rate Coefficients and Branching Ratios for Reactions of Organic Peroxy Radicals for Use in Automated Mechanism Construction. *Atmos Chem Phys* **2019**, *19* (11), 7691–7717. https://doi.org/10.5194/ACP-19-7691-2019.

(3) Nannoolal, Y.; Rarey, J.; Ramjugernath, D. Estimation of Pure Component Properties: Part 3. Estimation of the Vapor Pressure of Non-Electrolyte Organic Compounds via Group Contributions and Group Interactions. *Fluid Phase Equilib* **2008**, *269* (1–2), 117–133. https://doi.org/10.1016/J.FLUID.2008.04.020.

(4) Valorso, R.; Aumont, B.; Camredon, M.; Raventos-Duran, T.; Mouchel-Vallon, C.; Ng, N. L.; Seinfeld, J. H.; Lee-Taylor, J.; Madronich, S. Explicit Modelling of SOA Formation from α-Pinene Photooxidation: Sensitivity to Vapour Pressure Estimation. *Atmos Chem Phys* **2011**, *11* (14), 6895–6910. https://doi.org/10.5194/ACP-11-6895-2011.

(5) La, Y. S.; Camredon, M.; Ziemann, P. J.; Valorso, R.; Matsunaga, A.; Lannuque, V.; Lee-Taylor, J.; Hodzic, A.; Madronich, S.; Aumont, B. Impact of Chamber Wall Loss of Gaseous Organic Compounds on Secondary Organic Aerosol Formation: Explicit Modeling of SOA Formation from Alkane and Alkene Oxidation. *Atmos Chem Phys* **2016**, *16* (3), 1417–1431. https://doi.org/10.5194/ACP-16-1417-2016.

(6) Galeazzo, T.; Valorso, R.; Li, Y.; Camredon, M.; Aumont, B.; Shiraiwa, M. Estimation of Secondary Organic Aerosol Viscosity from Explicit Modeling of Gas-Phase Oxidation of Isoprene and α-Pinene. *Atmos Chem Phys* **2021**, *21* (13), 10199–10213. https://doi.org/10.5194/ACP-21-10199-2021.

(7) McVay, R. C.; Zhang, X.; Aumont, B.; Valorso, R.; Camredon, M.; La, Y. S.; Wennberg, P. O.; Seinfeld, J. H. SOA Formation from the Photooxidation of α-Pinene: Systematic Exploration of the Simulation of Chamber Data. *Atmos Chem Phys* **2016**, *16* (5), 2785–2802. https://doi.org/10.5194/ACP-16-2785-2016.

(8) Aumont, B.; Szopa, S.; Madronich, S. Modelling the Evolution of Organic Carbon during Its Gas-Phase Tropospheric Oxidation: Development of an Explicit Model Based on a Self Generating Approach. *Atmos Chem Phys* **2005**, *5* (9), 2497–2517. https://doi.org/10.5194/ACP-5-2497-2005.

(9) Verwer, J. G.; Blom, J. G.; Hundsdorfer, W. An Implicit-Explicit Approach for Atmospheric Transport-Chemistry Problems. *Applied Numerical Mathematics* **1996**, *20* (1–2), 191–209. https://doi.org/10.1016/0168-9274(95)00126-3.

(10) Verwer, J. G. Gauss–Seidel Iteration for Stiff ODES from Chemical Kinetics. *https://doi.org/10.1137/0915076* **2006**, *15* (5), 1243–1250. https://doi.org/10.1137/0915076.

(11) Seinfeld, J. H.; Pandis, S. N. Atmospheric Chemistry and Physics : From Air Pollution to Climate Change. **2006**, 1203.

(12) Takeuchi, M.; Berkemeier, T.; Eris, G.; Ng, N. L. Non-Linear Effects of Secondary Organic Aerosol Formation and Properties in Multi-Precursor Systems. *Nature Communications 2022 13:1* **2022**, *13* (1), 1–13. https://doi.org/10.1038/s41467-022-35546-1.

(13) Reid, J. P.; Bertram, A. K.; Topping, D. O.; Laskin, A.; Martin, S. T.; Petters, M. D.; Pope, F. D.; Rovelli, G. The Viscosity of Atmospherically Relevant Organic Particles. *Nature Communications 2018 9:1* **2018**, *9* (1), 1–14. https://doi.org/10.1038/s41467-018-03027-z.

(14) Zaveri, R. A.; Shilling, J. E.; Zelenyuk, A.; Liu, J.; Bell, D. M.; D, E. L.; Gaston, C. J.; Thornton, J. A.; Laskin, A.; Lin, P.; Wilson, J.; Easter, R. C.; Wang, J.; Bertram, A. K.; Martin, S. T.; Seinfeld, J. H.; Worsnop, D. R. Growth Kinetics and Size Distribution Dynamics of Viscous Secondary Organic Aerosol. **2017**. https://doi.org/10.1021/acs.est.7b04623.

(15) Zaveri, R. A.; Shilling, J. E.; Zelenyuk, A.; Zawadowicz, M. A.; Suski, K.; China, S.; Bell, D. M.; Veghte, D.; Laskin, A. Particle-Phase Diffusion Modulates Partitioning of Semivolatile Organic Compounds to Aged Secondary Organic Aerosol. **2020**. https://doi.org/10.1021/acs.est.9b05514.

(16) Li, Y.; A. Day, D.; Stark, H.; L. Jimenez, J.; Shiraiwa, M. Predictions of the Glass Transition Temperature and Viscosity of Organic Aerosols from Volatility Distributions. *Atmos Chem Phys* **2020**, *20* (13), 8103–8122. https://doi.org/10.5194/ACP-20-8103-2020.

(17) DeRieux, W. S. W.; Li, Y.; Lin, P.; Laskin, J.; Laskin, A.; Bertram, A. K.; Nizkorodov, S. A.; Shiraiwa, M. Predicting the Glass Transition Temperature and Viscosity of Secondary Organic Material Using Molecular Composition. *Atmos Chem Phys* **2018**, *18* (9), 6331–6351. https://doi.org/10.5194/ACP-18-6331-2018.

(18) Gordon, M.; Taylor, J. S. Ideal Copolymers and the Second-Order Transitions of Synthetic Rubbers. i. Non-Crystalline Copolymers. *Journal of Applied Chemistry* **2007**, *2* (9), 493–500. https://doi.org/10.1002/JCTB.5010020901.

(19) Dette, H. P.; Qi, M.; Schröder, D. C.; Godt, A.; Koop, T. Glass-Forming Properties of 3-Methylbutane-1,2,3-Tricarboxylic Acid and Its Mixtures with Water and Pinonic Acid. *Journal of Physical Chemistry A* **2014**, *118* (34), 7024–7033. https://doi.org/10.1021/JP505910W.

(20) Nguyen, T. B.; Nizkorodov, S. A.; Laskin, A.; Laskin, J. An Approach toward Quantification of Organic Compounds in Complex Environmental Samples Using High-Resolution Electrospray Ionization Mass Spectrometry. *Analytical Methods* **2012**, *5* (1), 72–80. https://doi.org/10.1039/C2AY25682G.

(21) Koop, T.; Bookhold, J.; Shiraiwa, M.; Pöschl, U. Glass Transition and Phase State of Organic Compounds: Dependency on Molecular Properties and Implications for Secondary Organic Aerosols in the Atmosphere. *Physical Chemistry Chemical Physics* **2011**, *13* (43), 19238–19255. https://doi.org/10.1039/C1CP22617G.

(22) Zobrist, B.; Marcolli, C.; Pedernera, D. A.; Koop, T. Do Atmospheric Aerosols Form Glasses? *Atmos Chem Phys* **2008**, *8* (17), 5221–5244. https://doi.org/10.5194/ACP-8-5221-2008.

(23) Gunthe, S. S.; King, S. M.; Rose, D.; Chen, Q.; Roldin, P.; Farmer, D. K.; Jimenez, J. L.; Artaxo, P.; Andreae, M. O.; Martin, S. T.; Pöschl, U. Cloud Condensation Nuclei in Pristine Tropical Rainforest Air of Amazonia: Size-Resolved Measurements and Modeling of Atmospheric Aerosol Composition and CCN Activity. *Atmos Chem Phys* **2009**, *9* (19), 7551–7575. https://doi.org/10.5194/ACP-9-7551-2009.

(24) Rose, D.; Gunthe, S. S.; Su, H.; Garland, R. M.; Yang, H.; Berghof, M.; Cheng, Y. F.; Wehner, B.; Achtert, P.; Nowak, A.; Wiedensohler, A.; Takegawa, N.; Kondo, Y.; Hu, M.; Zhang, Y.; Andreae, M. O.; Pöschl, U. Cloud Condensation Nuclei in Polluted Air and Biomass Burning Smoke near the Mega-City Guangzhou, China - Part 2: Size-Resolved Aerosol Chemical Composition, Diurnal Cycles, and Externally Mixed Weakly CCN-Active Soot Particles. *Atmos Chem Phys* **2011**, *11* (6), 2817–2836. https://doi.org/10.5194/ACP-11-2817-2011.

(25) Petters, M. D.; Kreidenweis, S. M. A Single Parameter Representation of Hygroscopic Growth and Cloud Condensation Nucleus Activity. *Atmos Chem Phys* **2007**, *7* (8), 1961–1971. https://doi.org/10.5194/ACP-7-1961-2007.

(26) Kuwata, M.; Martin, S. T. Phase of Atmospheric Secondary Organic Material Affects Its Reactivity. *Proc Natl Acad Sci U S A* **2012**, *109* (43), 17354–17359. https://doi.org/10.1073/PNAS.1209071109.

(27) Li, Y.; Pöschl, U.; Shiraiwa, M. Molecular Corridors and Parameterizations of Volatility in the Chemical Evolution of Organic Aerosols. *Atmos Chem Phys* **2016**, *16* (5), 3327–3344. https://doi.org/10.5194/ACP-16-3327-2016.

(28) Isaacman-Vanwertz, G.; Aumont, B. Impact of Organic Molecular Structure on the Estimation of Atmospherically Relevant Physicochemical Parameters. *Atmos Chem Phys* **2021**, *21* (8), 6541–6563. https://doi.org/10.5194/ACP-21-6541-2021.

(29) Li, Y.; Pöschl, U.; Shiraiwa, M. Molecular Corridors and Parameterizations of Volatility in the Chemical Evolution of Organic Aerosols. *Atmos. Chem. Phys* **2016**, *16*, 3327–3344. https://doi.org/10.5194/acp-16-3327-2016.

(30) Malloy, Q. G. J.; Nakao, S.; Qi, L.; Austin, R.; Stothers, C.; Hagino, H.; Iii, D. R. C.; Cocker Iii, D. R. Real-Time Aerosol Density Determination Utilizing a Modified Scanning Mobility Particle Sizer-Aerosol Particle Mass Analyzer System. *Aerosol Science and Technology* **2009**, *43* (7), 673–678. https://doi.org/10.1080/02786820902832960.

(31) Nakao, S.; Tang, P.; Tang, X.; Clark, C. H.; Qi, L.; Seo, E.; Asa-Awuku, A.; Iii, D. C. Density and Elemental Ratios of Secondary Organic Aerosol: Application of a Density Prediction Method. https://doi.org/10.1016/j.atmosenv.2012.11.006.

(32) Faiola, C. L.; Buchholz, A.; Kari, E.; Yli-Pirilä, P.; Holopainen, J. K.; Kivimäenpää, M.; Miettinen, P.; Worsnop, D. R.; Lehtinen, K. E. J.; Guenther, A. B.; Virtanen, A. Terpene Composition Complexity Controls Secondary Organic Aerosol Yields from Scots Pine

Volatile Emissions. *Scientific Reports 2018 8:1* **2018**, *8* (1), 1–13. https://doi.org/10.1038/s41598-018-21045-1.